VOLUME MEASUREMENT BY ULTRASOUND AND MRI IMAGING

Apr. 16, 2016

CHU YUNWEN (DARREN) 3035181217

LV RUYI (ZACH) 3035142560

YIP GWING KEI (GWINKY) 3035176303

INTRODUCTION

Ultrasound is an imaging method, which uses high-frequency sound waves to view organs like heart, blood vessels, kidneys and liver. It is also commonly used to view the fetus during pregnancy. Radiation exposure is avoided compared to X-ray imaging. It is also popular for it is noninvasive, relatively safe, portable and cheap. [1] Actual nature, structure and acoustic characteristics of the tissue are measured in ultrasound. Central Processing Unit (CPU) of ultrasound, which includes the processor, memory, and amplifier is the most important component of ultrasound machine. The CPU process the information and form the ultrasound images. Transducer Pulse Controls changes the frequency and duration of ultrasound. This allows the change of scanning mode. [2] In clinical application, different transducer probes are used under different situations to obtain the best images. For example, phased type transducer is usually used in cardiac application, transesophageal, abdominal application and brain diagnosis. [3] Ultrasound machine also have display, keyboard, disk storage and printer.

Different modes of sonography are used in ultrasound imaging, such as A-mode, B-mode, C-mode, Doppler mode, pulse inversion mode and harmonic mode. Every mode have its own applications in clinical use. When imaging the structures of heart, ultrasound is regarded as the predominant method. Echocardiography, which is the sonogram of heart creates images that can help in heart disease detection and determination. Doppler echocardiography can help analyze the blood flow in heart. [4] Resolution is always a concern in medical imaging, both spatial and temporal resolution. In ultrasound, the axial resolution is determined by the wavelength as well as number of cycles in the pulse. Lateral resolution, however, is determined by wavelength, focal length and aperture size. Other than spatial resolution, temporal resolution is also vital factor to be considered in ultrasound. It is determined by sound velocity, depth, number of scan lines per frame and transmit foci. [1]

Magnetic resonance imaging (MRI) is also a non-invasive, relatively safe medical imaging modality. MRI creates contrast by comparing tissue properties of T1-relaxation, T2-relaxation and proton density. [4] MRI consists of four main components. The main magnet is used to create a basic and constant magnetic field, which leads to the magnetic vector. Protons align themselves along the magnetic field and precess around at the Larmor frequency. RF coils are mainly for transmitting RF pulse and receiving signals. The RF pulse make some protons transform into their high energy states. Proton becomes synchronized and the T1 and T2 relaxation time can be measured. The gradient coils produce positive and negative pulses in x, y and z axis. This enables the MRI to gain position information in order to localize the MR images in three dimensions. [1][2] MRI depends on nuclei properties to form images. Protons spin under with magnetic fields added. RF pulse generated creates another magnetic field and flips the net magnetization into transverse plan. When is RF switched off, time taken to return to part of initial magnitude of magnetization is measured. These information are then collected to form contrast in MRI images. [1]

MRI is usually considered a powerful tool for viewing brain structures. Spatial resolution in MRI is the imaging voxel size of MRI machine, which is determined by matrix size, the field-of view and the slice thickness. The resolution is actually different in three directions. [1]

	MRI	Ultrasound
Physical Quantity measured	Proton density, T1 relaxation and T2 relaxation	Actual nature, structure and acoustic characteristics
What can be adjusted from the control panel/software	Direction of scanning, T1 or T2 weighted	Brightness, gain in specific areas (TGC), focus position, focus zone, frequency, modes, dynamic range (compression) and etc.
Key factors that determine the acquisition rate (or, frame rate)	Depth, number of transmit foci, number of scan lines per frame, sound velocity (presumed constant)	Repetition time, number of cycle repetitions (quality requirement), reconstruction time and etc.
Spatial resolution	Matrix size, the field-of-view and the slice thickness.	Wavelength, number of cycles in the pulse, focal length, aperture size
Image contrast	The repetition time and the echo time	The nature of tissue, contrast media
Safety	Vital to remove all metallic belongings in advance No radiation harm	No evidence of harm
Volume accuracy in this lab	Better	Good

MATERIALS AND METHODS

Simpson's Rule: In this lab we choose both ellipsoid volume and Simpson's rule to evaluate the volume of left ventricle. The modified Simpson's approximation is the most accurate current-existing math method to estimate left ventricle volume. Though the trabeculated endocardial surface may lead to the small change of the actual volume, the approximation is widely used. [5] The left ventricle shows an oval or approximately circular outline in its transverse section. When using the Simpson's rule, the total left ventricle volume is calculated by approximating the ventricle with a stack of elliptical disks. Other methods are also available in this process. [6] Detailed information are shown in the figure.

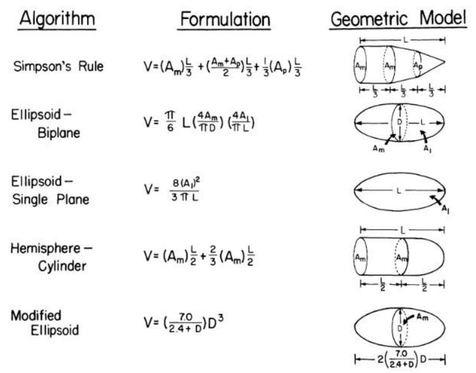

Figure 1 (retrieved from [6]) (Simpson's rule denoted as formula y in the rest of the report)

Ellipsoid Volume: The volume bounded by the ellipsoid is $V = \frac{4}{3}\pi abc$ (denoted as formula x in the rest of the report) and the definition for ellipsoid is a closed quadric surface that is a three-dimensional analogue of an ellipse. Ellipsoid exists commonly in nature, but in this case it doesn't seem to be so fit for estimating left ventricle volume, at least for the mold we make.

B-Mode: In ultrasound imaging, we used real-time B-mode to acquire the data. Unlike other mode, B mode display the brightness representing the ultrasound echo. This method is best when measuring areas like the case in this lab. For the same principle, B-mode is also used for real-time guidance when injecting needle.

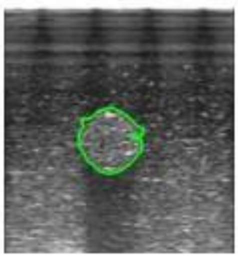

Figure 2. B-mode

Hilbert Transform: When analyzing the ultrasound data, Hilbert transform was employed. The Hilbert transform extend real signal into the complex plane. It cases where high sample rates and high digital capabilities appear, Hilbert transform is commonly used. This math function shifts the input by 90 degrees in phase. The modification of the raw signal allow the combination of signals. The signals can fit in the ripples of others' and envelope magnitude can be estimated. [7]

MRI Data: Six groups of MRI data are collected in each case. The first group contain positioning information. Geometric planning are completed using information from the second and third groups, the second for transverse direction and the third for longitudinal direction. The fourth group exhibits T2-weighted final image and the fifth group exhibits T1-weighted image. The last group contain T2-weighted image with short echo time. The ET for the sixth group is 17.5ms and for fourth group is 70ms.

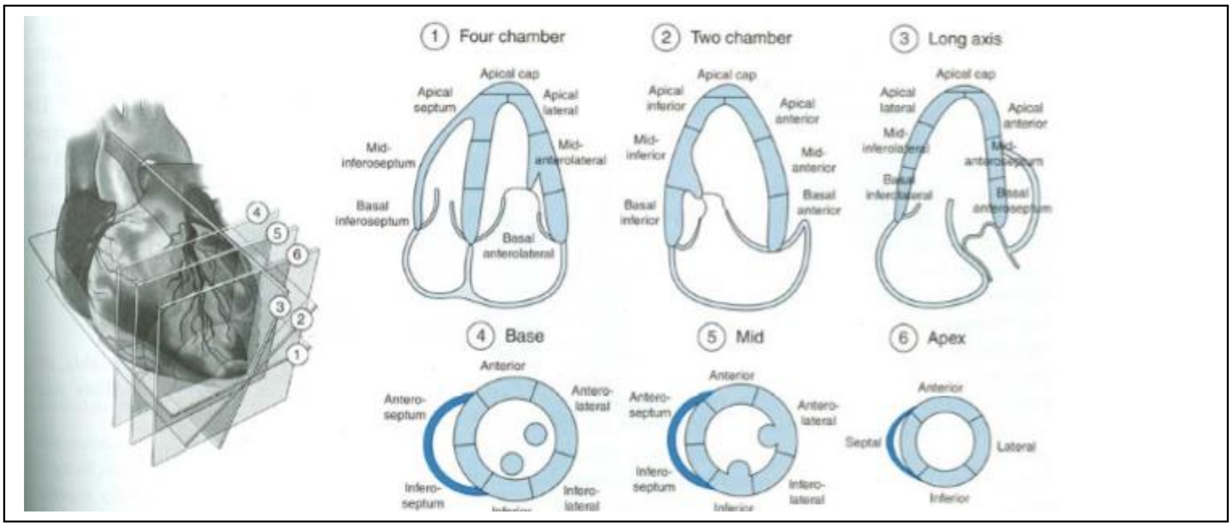

Figure 3 Retrieved from [8]

RESULTS

As seen from the given figure 3, 1-3 are taken in a long parasternal orientation while 4-6 in the short parasternal orientation. By rotating the imaging angle for 1-3, (1) gives a four chamber view of all the left and right atria and ventricles as well as their respective valves, (2) gives a two chamber view of the left atrium and ventricle, (3) also gives the view of the left side in addition to the proximal end of the aorta and a bit of the right ventricle.

Among 4-6, (6) is the view taken closest to the apical cap, followed by (5) then (4). (6) shows mainly the left ventricle tip with a bit of the right ventricle, (5) shows a larger lumen with the two papillary muscles emerging out of the periphery, (4) shows an even larger lumen with both muscles separated from the periphery.

Ultrasound can also see weaker signals such as blood using the Doppler mode. By transmitting and receiving the ultrasound beam at a known angle, one can calculate the velocity of the moving objects by measuring the phase shift of the received signal, which is independent from the amplitude of the signal thus allows measuring even weak signals. By aligning the beam transmitter closer to the direction of object movement and increasing the ultrasound frequency, a larger Doppler frequency can be measured.

$$\text{Doppler equation: } v = \frac{f_D \times v_0}{2 \times f_0 \times \cos\alpha}$$

Question 2.1: This is because ultrasound wave cannot travel very well in air. So any bit of air between the array probe and the patient's skin may disturb the outcome of ultrasound imaging. The ultrasound gel, lubricating the skin, ensure a tight connection between the skin and array probe.

Question 2.2:

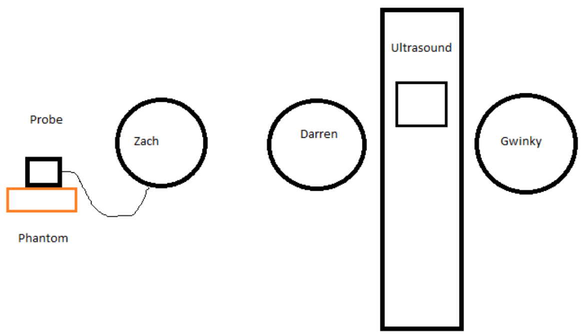

Question 2.3:

B-mode Images obtained by matlab (refer to appendix 1.1)

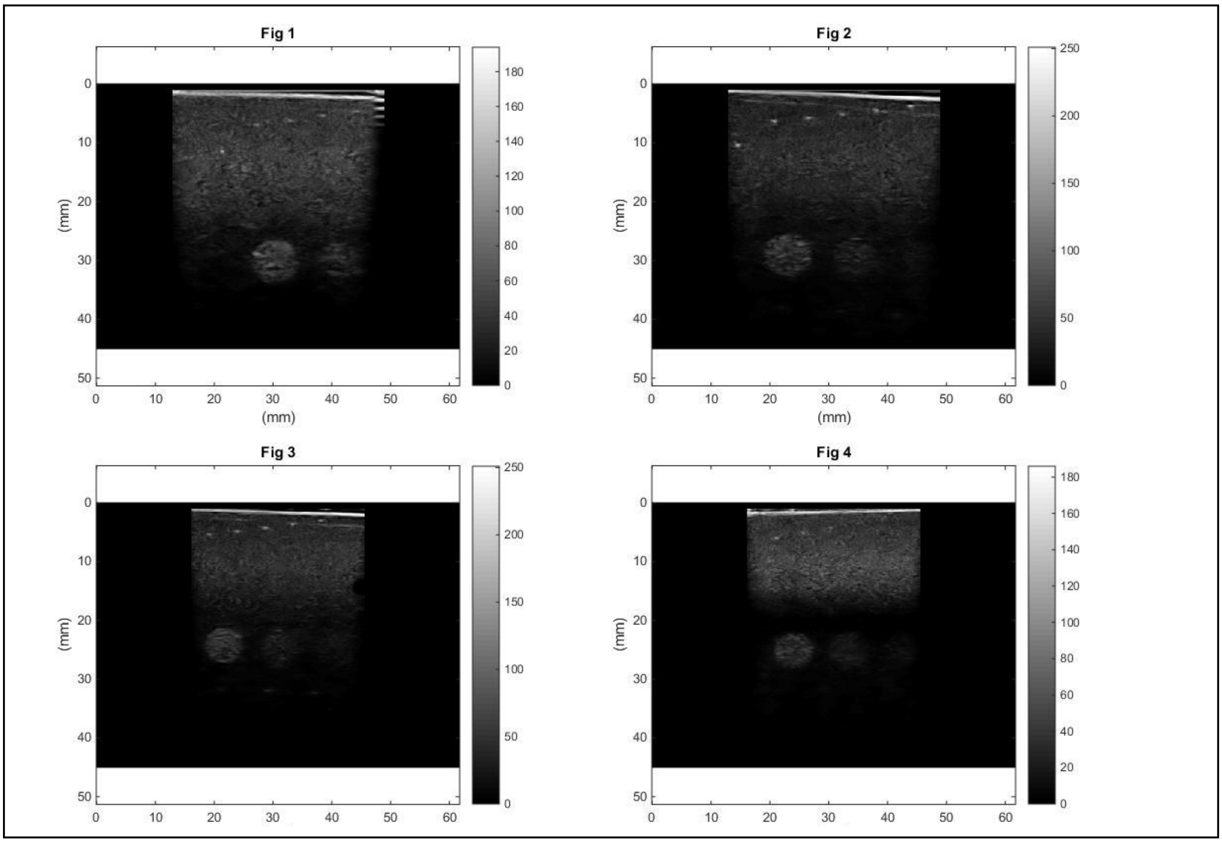

Figure 1-4 with the following parameters:

Figure	Frequency (MHz)	Depth (mm)	TGC
1	6.6	45	N
2	10	45	N
3	10	55	N
4	10	55	Y

Frequency (1 & 2): Figure 2 (10MHz) has a better resolution than figure 1 (6.6MHz), but with a smaller depth. This is because a higher frequency wave increases both axial and lateral resolution as given by the equations,

$$\text{axial resolution} = \frac{m}{2f_0} v_0 = \frac{m\lambda}{2},$$

$$\text{lateral resolution} = 0.384\lambda F_{\#} = 0.384\lambda \frac{F}{D}$$

while it is also more prone to attenuation by scattering and absorption by substances, that is the loss of amplitude thus the amount of energy further down the axial axis.

Depth (2 & 3): Figure 2 (45mm) has a lower depth than figure 3 (55mm). While figure 3 gives a wider view of the same object than in figure 2, due to the limited pixels number, the object in figure 3 has a lower pixel resolution when scaled to the same size as in figure 2. Therefore figure 2 can give more details of the object than 3.

TGC gain (3 & 4): The TGC applied to figure 4 is shown on the right.

A darker line can be observed in the middle of figure 4 where TGC is not applied. Since TGC refers to time gain compensation, that is the amplification of the return signal aimed to compensate the loss by attenuation down the depth, the darker line indicates a weaker signal received compared to the other sections. Figure 3 has a full, uniform TGC gain, thus the image is clearer.

Question 2.4: The images are read using matlab (refer to appendix 1.2).

Since all images have pixels dimension (y*x) =356*488 (appendix 1.3) and an actual depth of 45mm, the resolution is given as 45/356 = 0.126mm.

Question 2.5: The Hilbert transform is performed by matlab (appendix 1.2).

The transformed matrix has a dimension of 2336x256, same as the chosen rf image. However the transformed matrix carries complex numbers instead.

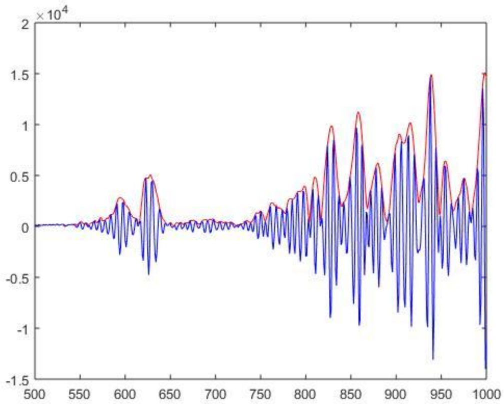

Blue: raw data of a fixed x; Red: Amplitude of Hilbert transform.

Question 3.1: The ground truth volume is derived from the mold design from Sketchup, given as 2749.963mm^3.

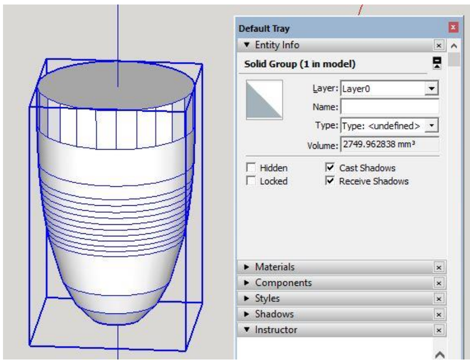

Question 3.2 & 3.3: Using imageJ, the average maximum area of the transverse and horizontal plane is measured.

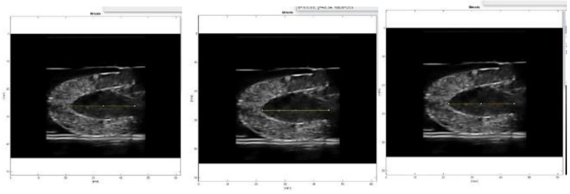

Results

File Edit Font Results

	Area	Mean	Min	Max	Angle	Length
1	1.664	27.429	11.041	50.492	0.000	22.663
2	1.686	33.498	14.883	69.975	0.000	22.990
3	1.669	32.494	15.355	68.292	0.000	22.772

Top: Left: Bmode; Right: raw data;

Bottom: Left: Hilbert transform; Right: dB scaled Hilbert;

A similar B-mode image can be produced from the raw data using Hilbert transform.

A dB scale is performed for clearer image by removing lower frequency.

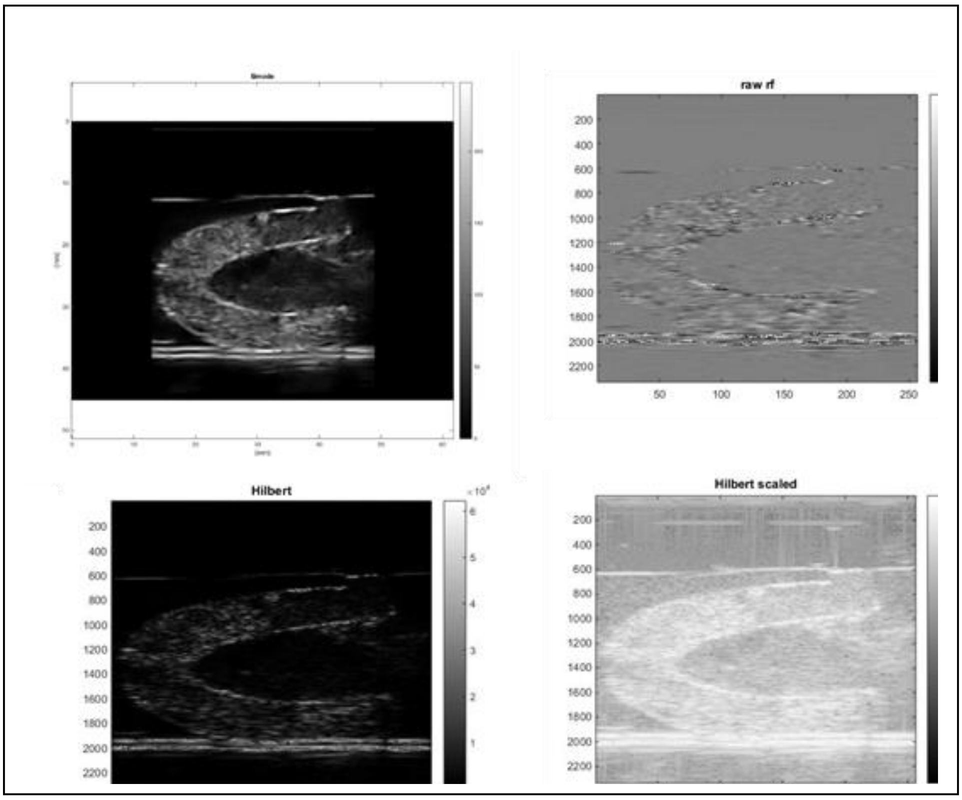

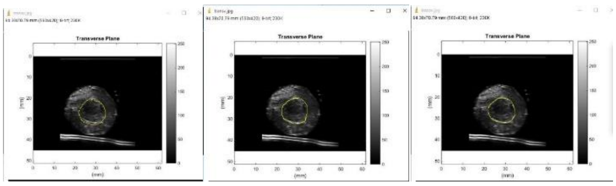

	Area	Mean	Min	Max	Angle	Lengt
1	117.798	48.040	0.000	255.000	0.000	0.000
2	114.673	48.265	0.000	255.000	0.000	0.000
3	115.213	47.500	0.000	255.000	0.000	0.000

Data	Length c (mm)	Area a*b*pi (mm^2)
1	22.663	117.798
2	22.99	114.673
3	22.772	115.213
Average	22.80833333	115.8946667
volume=	1762.242793	

Assuming the phantom as a half ellipsoid, volume=4/3*pi*abc/2; Area of ellipse=pi*ab

Volume=4/3*pi*abc/2 = 4/3 *c *area/2 =1762.242793mm^3

The result is smaller than the ground truth with an error of -35.9%. Boundary tracing using matlab is also tried instead of using imageJ. However a clear boundary cannot be determined.

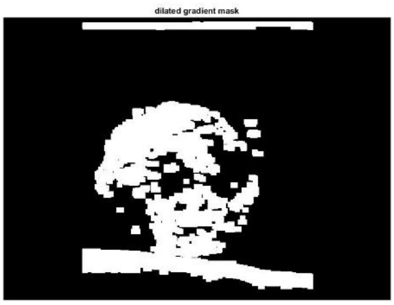

Question 3.4: Simpson's rule is used to find the volume.

$$V=(A_m)\frac{L}{3}+\left(\frac{A_m+A_p}{2}\right)\frac{L}{3}+\frac{1}{3}(A_p)\frac{L}{3}$$

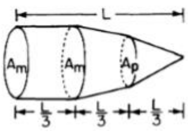

z length	Area (mm^2)	simpson (mm^3)
0	115.8946667	769.5671051
1/3	86.549	504.4747167
2/3	46.159	116.9788731
		1391.020695

Assuming the first two sections as a cylinder and the last as a cone, the volume is found as 1391.020695mm^3. The result has an error of -49.4%, which is worse than that by simple calculation of a half ellipsoid volume.

Question 2.1: The imaging mechanism of MRI and ultrasound are different. The bulk transparent material and plastic tube are used for better preservation of PVA phantom. Since ultrasound acquire information from the echoes of sound waves, the plastic tube will indeed disturb the imaging of the phantom, decreasing the clarity. MRI depends on the spin of the protons and it needs to fix the phantom in a certain position, so the plastic tube and bulk material don't need to be removed.

In this experiment, multiple imaging planes were taken, but only three planes were used in the calculation, which are three planes needed in Simpson's rule. To apply the modified Simpson's rule, only three transverse planes with equal distance need to be obtained and measured. But if we want to conduct more accurate calculation, other measuring planes may be needed for calculation and determination.

Question 2.2: Sequence T2 is used. As described in section II, the respective images from sequence 2-6 is shown as below:

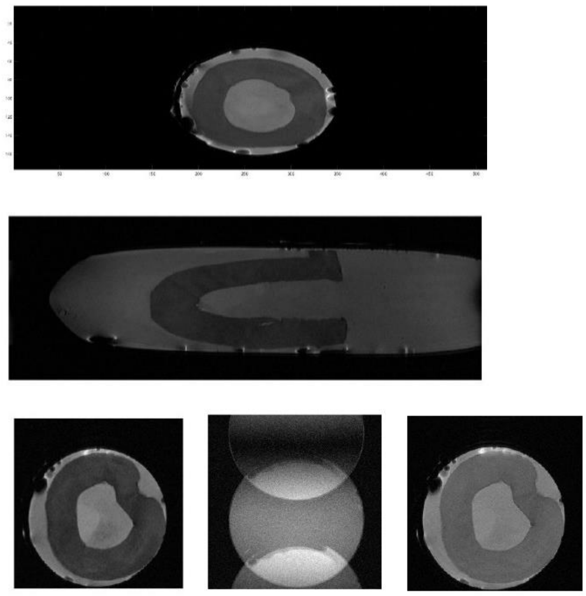

(Top:2,3;Bottom:4,5,6;) Since 2-3 are just for geometric planning, parameters are not properly set for actual imaging.

Sequence	Weighting	TE (ms)
4	T2	70
5	T1	70
6	T2	17.5

Since the image 4 gives a clearer image than 5 and has a higher contrast than 6, its parameters are chosen for imaging. It is T-2 weighted with a longer TE (70ms). As the phantom composition is rich of water and T2 images give a darker grey color to fluid that contrasts the surrounding bright color, it has the optimal imaging circumstance. A longer TE than image 6 also gives better T2 features.

Question 2.3: The images taken in sequence 4 has the following parameters:

DIM: [256 256 23]

reconDIM: [256 256 23]

FovCm: [3.2000 3.2000 3.4500]

SliceThickMm: []

VOX: [0.1250 0.1250 1.5000]

TR: 4

NEX: 1

Ncoil: 1

shift: -18

TE: 70ms

The scan time depends on how high the resolution is and the number of images taken. From the matrix size [x y z], larger x and y means more pixels and z means more images, so the higher the longer it takes.

Fov is the image actual length, and vox is simply fov/matrix size. Therefore smaller fov gives a smaller image but better resolution for reconstruction.

TR is the repetition time and TE is the echo time. Together their length determines the sequence thus the contrast of the image. The common type is T1 and T2, where T1 requires short TE and TR and T2 requires long TE and TR. Therefore TE and TR give different contrast of image. T1 may also take longer than T2 as T2 relaxation occurs whenever T1 relax, but not vice versa. So the scan time is longer for T1, which is determined also by shorter TE and TR.

Comparing image 4 and 6, both has the same TR=4ms but different TE=70ms and 17.5ms respectively. Since a T2 image is necessary a sequence trying to minimize T1 effect, a short TE will allow little time for T2 decays difference to be noticeable. Therefore the signal difference is reduced, as well as the contrast.

Question 2.4: The image data is read using matlab (refer to appendix 2.1).

Images of different sequences are shown in q2.2.

Images of sequence 4 along z axis are shown below:

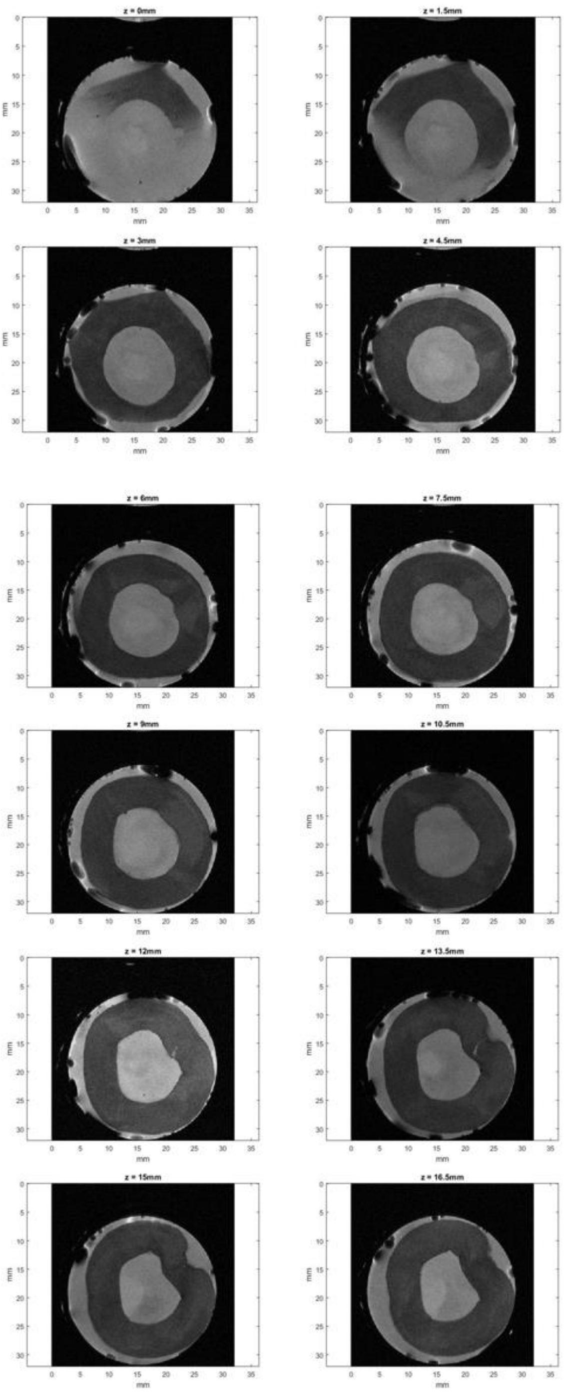

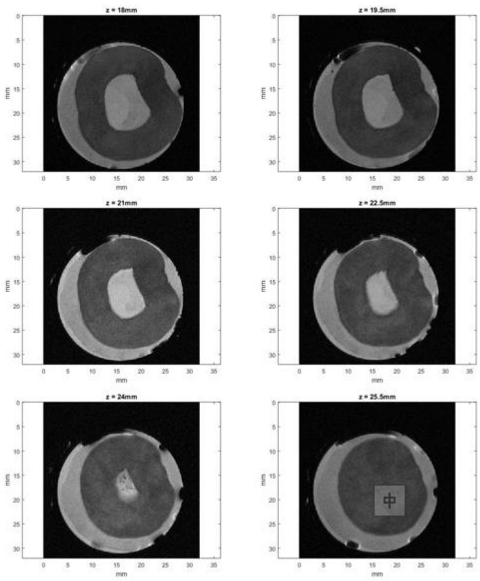

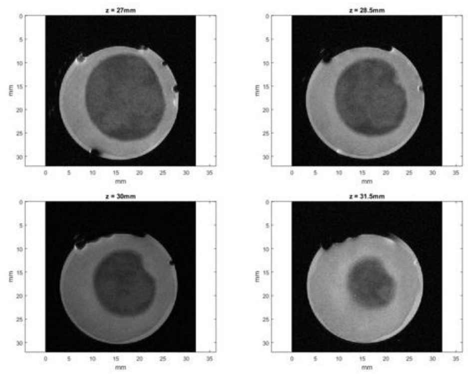

Each image has a pixel resolution of 256*256 and an actual length of 32mm. The resolution is given by 32/256=0.125mm.

Using imageJ, the area of the image when z=0, z=9, z=18 is found. The ellipsoid equation and Simpson's method is then used to find the volume.

z(mm)	imageJ(mm^2)	Simpson(mm^3)	ellipsoid(mm^3)
0	132.489	1103.8095	2252.313
1.5	132.489		
3			
4.5			
6			Green=final volume
7.5			
9	112.802	873.981	
10.5			
12			
13.5			
15			
16.5			
18	81.416	203.54	
19.5			
21			
22.5			
24			
25.5	0	2181.3305	
27			
28.5			
30			

The error of the ellipsoid equation is -18.1% and the Simpson's method is -20.7%.

DISCUSSION

A. Major Results

As introduced in the former section, the volume measurements of the phantom by ultrasound and MRI can be summarized in the following table:

Approaches of volume measurements and calculations	Measured volumes of the heart phantom (mm^3)
Ultrasound—Image J—Simpson's rule	1391.020695
Ultrasound—Image J—Ellipsoidal approach	1762.242793
MRI—Image J—Simpson's rule	2181.3305
MRI—Image J—Ellipsoidal approach	2252.313
MRI—SOBEL—Multiple image planes (i.e. 18 planes)	2392.221344
Ground Truth	2749.962838

Figure 4

B. Error Analysis

First of all, from the results in the former section, the heart phantom we made is suspected to be significantly smaller than that we designed. This may be the result of post-trimming of the phantom after construction, which we are not so sure how it was done. The accuracy of the 3D printing machine may also account for the differences between the measured volumes of the heart phantom (by both ultrasound and MRI) and the ground truth.

As shown in Figure 4, the volume of the heart phantom measured by ultrasound and calculated by ellipsoidal approach is statistically significantly different from (or smaller than) the ground truth by 35.9%. There are three major errors:

a) Image Position (IP) Error:

When computing the measured volume of the heart phantom, proper algorithm will be applied. Most importantly, specific planes are required to be imaged in all these algorithms. However, since the volume measurements of the heart phantom by ultrasound are done by freehand scanning, the planes to be imaged may not be the desired planes and thus errors will be involved. For example, if Simpson's Rule is used, three specific cross sections with equal spatial separation are needed to be imaged (as shown in Figure 5). Nevertheless, the plane to be imaged can be tilted (i.e. A_a) or even distant from (i.e. A_b) the desired image plane (i.e. A_m), and this will significantly affect the volume of the heart phantom calculated by using Simpson's Rule. Therefore, there is IP error in this case.

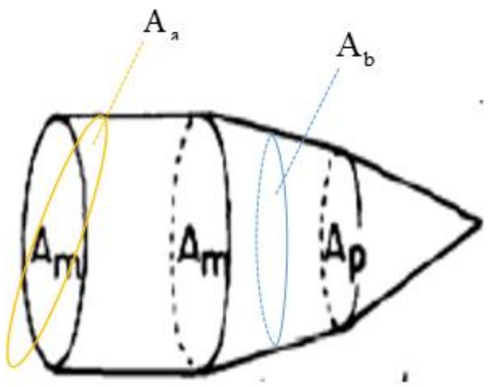

Figure 5. *Illustration of how the plane to be imaged can be titled or distant from the desired image plane.*

b) Geometric Assumption (GA) Error:

In section III, although two different algorithms are employed to calculate the measured volumes of the phantom, both of them are based on certain geometric assumptions. For formula x, the heart phantom is assumed to be ellipsoidal while for formula y, the heart phantom is assumed to be the sum of a cylinder, a truncated cone and another cone. However, the geometry of the heart phantom is neither perfectly ellipsoidal nor the sum of a cylinder, a truncated cone and another cone. Therefore, GA error is involved in both cases.

Nevertheless, a special observation to be noted here is that the volume of the heart phantom calculated by using formula x (i.e. 1762.242793 mm^3) is nearer to the ground truth (i.e. 2749.962838 mm^3) than that by using formula y (i.e. 1391.020695 mm^3). The possible reason is that obviously, the geometry of the heart phantom is better approximated as an ellipsoid rather than the sum of a cylinder, a truncated cone and another cone (as shown in Figure 6).

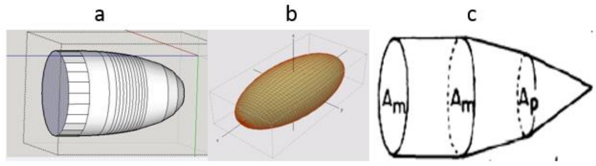

Figure 6. *The geometries of the heart phantom (a), an ellipsoid (b) and the sum of a cylinder, a truncated cone and another cone (c).*

c) Boundary Tracing (BT) Error:

When calculating the area of chosen cross section of the heart phantom, a software called Image J will be utilized to trace the boundary by drawing a red line based on the observation by naked eyes so that the area bounded by the red line will be automatically computed. However, due to the presence of speckle noises, there will be limited contrast resolution of the images taken by ultrasound. Therefore, the edges will be unclear and difficult to be identified. As a result, the calculated bounded area may be deviated from the authentic area of the cross section and thus, BT error is involved in this case.

On the other hand, as shown in Figure 4, the volume of the heart phantom measured by MRI and calculated by ellipsoidal approach is also statistically significantly different from (or smaller than) the ground truth by 18.1%. There are again three major errors:

d) Image Position (IP) Error:

Just like part a), there is also IP error in this case because the plane to be imaged may be tilted or even distant from the desired image plane. However, the IP error in this case will probably be smaller than that in part a) as image plane planning is done by using a computer before carting out imaging. Although the plane to be imaged still may not be exactly the desired image plane, it will be more accurate than freehand scanning.

e) Geometric Assumption (GA) Error:

Basically, the explanation in this part is exactly the same as stated in part (b). There is GA error in this case because the geometry of the heart phantom is neither perfectly ellipsoidal nor the sum of a cylinder, a truncated cone and another cone. In addition, the results (as shown in Figure 4) also show that the volume of the heart phantom calculated by using formula x (i.e. 2252.313 mm^3)

is nearer to the ground truth (i.e. 2749.962838 mm^3) than that by using formula y (i.e. 2181.3305 mm^3).

f) Boundary Tracing (BT) Error:

For MRI, although the image quality in terms of signal to noise ratio and contrast resolution is better than that for ultrasound, BT error is still involved. When tracing the boundary by using Image J, since the red line is drawn based on the observation by naked eyes, the bounded area may be deviated from the authentic area of the cross section due to human errors. However, the BT error in this case will probably be smaller than that in part c) because the edges in images taken by MRI are clearer and more easily traced than that taken by ultrasound. As a result, the bounded area in this case will be nearer to the authentic area of the chosen cross section.

All in all, errors in volume measurements of the heart phantom by both ultrasound and MRI come from both inter-operator variabilities (i.e. IP error and BT error) and intra-operator variability (i.e. GA error).

Besides, the results (as shown in Figure 4) show that the volume of the heart phantom measured by using MRI (i.e. 2252.313 mm^3) is nearer to the ground truth (i.e. 2749.962838 mm^3) than that by using ultrasound (i.e. 1762.242793 mm^3) (both are calculated by ellipsoidal approach). That means MRI is better than ultrasound in measuring the volume of the heart phantom. This is a reasonable result because from the above error analysis, although the same GA error is involved in the volume measurements of the heart phantom by both ultrasound and MRI, the IP error and BT error in the latter one is smaller than that in the former one.

C. Improvements of the Experiment

Ultrasound:

a) Usually, in clinical setting, ultrasonography can only be performed by expertise because the measurement is done by freehand scanning. That means only very experienced technician can accurately image the desired planes. For a layman to measure the volume of heart phantom by using ultrasound, IP error will probably be very large because the plane to be imaged will likely be tilted or even distant from the desired image plane. Therefore, one of the methods of improvement is that volume measurements of the heart phantom can be done after ample practice so that IP error can be reduced. In addition, regarding IP error, another way of to reduce IP error is to offer a 3-dimensional reference frame [9].

b) Regarding GA error, the way to improve is to increase the number of cross sections to be imaged. No matter formula x or formula y is used to compute the measured volume of the heart phantom, only three image planes are relied on and thus the dependence on geometric assumptions is large. However, taking Simpson's Rule as an example, the reliance on geometric assumption (i.e. the object to be imaged is assumed to be the sum of a cylinder, a truncated cone and another cone) can be reduced by increasing the cross sections to be imaged (i.e. with smaller spatial separations between cross sections to be imaged) as more planes are taken account for volume calculation (the volume will be the summation of multiplying the appropriate cross-sectional areas with the section thickness). As a result, GA error can be reduced.

c) This time, since the edges in the images are unclear and difficult to be identified because of the presence of speckle noise, MATLAB functions, such as SOBEL cannot be employed to trace the boundary so as to reduce the BT error by getting a more accurate area of a chosen cross section. Although several methods have been proposed to reduce the speckle noise, nearly all of them have undesirable disadvantages. For example, some small details of the image will be lost after applying adaptive filters [10].

However, a recent research has proposed a better approach to remove the speckle noise (as shown in Figure 7). Briefly speaking, the idea is that firstly, if the original image has an extremely low contrast, the areas with lower local contrast can obtain a higher contrast by performing histogram equalization [10]. Then, based on the assumption that speckle noise is multiplicative, it can be transformed to be additive by performing logarithmic transformation. After that, by applying diffusion tensor along the direction of greatest coherence, the broken boundaries of the structures in the image can be reconnected [10]. Finally, by performing exponential transformation, the image will be restored in the linear x-y space. As a result, an image with reduced speckle noise can be obtained. Then, SOBEL may be able to be used for tracing the boundaries so that BT error can be reduced.

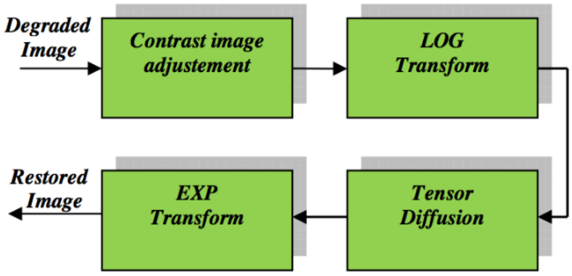

Figure 7. *Block diagram of the proposed model.* (Benzarti et al., 2013)

MRI:

d) Since image plane planning can be done by using computer before undergoing imaging, IP error may be not large indeed. However, improvement can still be done to further reduce IP error. For example, a better algorithm or software can be employed so that the accuracy of imaging the desired planes can be enhanced. As a result, IP error will be reduced.

e) Basically, regarding GA error, the method of improvement is exactly the same as that stated in part b). The key idea is that by increasing the number of planes to be imaged, the reliance on geometric assumptions can be reduced. As a result, GA error will be decreased. The corresponding evidence of improvement will be provided in part f).

f) For MRI, as the image quality in terms of signal to noise ratio and contrast resolution is better than that for ultrasound, the edges in the image are clearer and more easily identified. In this case, MATLAB functions, such as SOBEL can be utilized to trace the boundaries. This can eliminate the human errors in drawing the boundary curve due to observation by naked eyes. Then, the bounded area will be nearer to the authentic area of the chosen cross section. As a result, BT error can be reduced.

In order to verify the effectiveness of this improvement, a volume measurement of the heart phantom by using MRI is done by taking 18 image planes for calculating the volume and using SOBEL to trace the boundary of the chosen cross section (as shown in Figures 8 and 9). The result shows that it (i.e. 2392.221344 mm^3) is nearer to the ground truth (i.e. 2749.962838 mm^3) than the measured volume of the heart phantom done by using formula x and Image J (i.e. 2252.313 mm^3) (as shown in Figure 4). This provides evidence that the approaches mentioned above can effectively improve the accuracy of volume measurement of heart phantom by reducing the GA error and BT error.

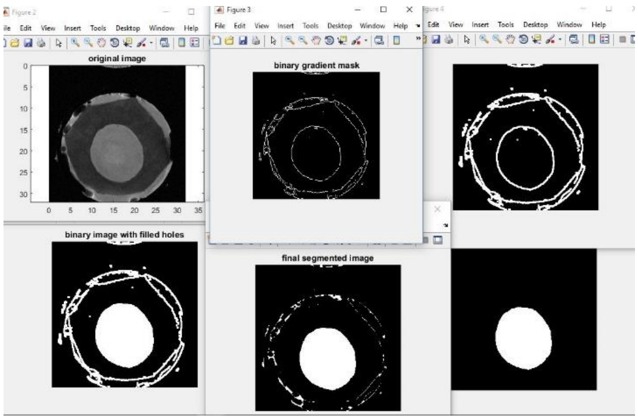

Figure 8. *Processes of boundary tracing of images by using SOBEL. (Top left to top right: original image, Sobel image and dilated image; Bottom left to bottom right: filled image, smoothed image and segmented image)*

z(mm)	Area(pixels)BT	Area(mm^2)	Volume segment(mm^3)		MRI index
0	N/A	132.489	198.7335		1
1.5	N/A	132.489	198.1206563		13
3	8427	131.671875	194.8945313		2
4.5	8204	128.1875	187.3828125		14
6	7786	121.65625	177.5039063		3
7.5	7361	115.015625	171.4804688		15
9	7272	113.625	168.2578125		4
10.5	7086	110.71875	163.875		16
12	6898	107.78125	156.9492188		5
13.5	6495	101.484375	148.6640625		17
15	6191	96.734375	139.9335938		6
16.5	5750	89.84375	127.0546875		18
18	5092	79.5625	110.6484375		7
19.5	4350	67.96875	93.28125		19
21	3610	56.40625	73.921875		8
22.5	2698	42.15625	61.55859375		20
24	2555	39.921875	19.9609375		9
25.5	0	0	2392.221344	=volume	21
27	0	0			10
28.5	0	0			22
30	0	0			11
31.5	0	0			23
33	0	0			12

Figure 9. *The data of the volume calculation of the heart phantom by using SOBEL and ellipsoidal approach.*

D. Clinical Significance, Real Situation and Usual Practice

The clinical significance of measuring the volume of left ventricle is that this can be used in the assessment of coronary artery diseases with infraction, vavular heart diseases and left ventricular hypertrophy [11].

In theory, if the heart phantom is replaced by a real heart, then the volume of the left ventricle of the real heart can be measured. However, the measurement will indeed be much harder in clinical situation due to several reasons:

a) Originally, in the experiment, the heart is static so that it would be easier for us to image the desired planes to be imaged. However, in reality, the heart is beating. If 2D echocardiography is used to measure the left ventricular volume, the IP errors will be very large because by freehand scanning, it is extremely difficult for the technician to image exactly the desired planes to be imaged of a beating heart.

b) For patients with cardiovascular diseases, such as myocardial infraction, there will be variations in geometries of the heart [9, 11]. As a result, some commonly used volume calculation algorithms like Simpson's rule can no longer accurately calculate the left ventricular volume since the geometric assumption (i.e. the object to be imaged is assumed to be the sum of a cylinder, a truncated cone and another cone) now cannot approximate the geometries of the hearts well. As a result, the GA error may be very large in clinical situation

c) Originally, in the experiment, the volume of the heart phantom can be directly measured. However, in reality, heart will be inside the body and in order to measure the left ventricular volume, the emitted ultrasound waves need to penetrate skins, bones or even organs. Therefore, the received ultrasound waves would suffer from large attenuation and the images taken would also be noisier. As a result, due to the lower signal to noise ratio of the images, BT error will be larger because the boundaries in this case are less clear and thus more difficult to be traced.

In order to tackle the difficulties mentioned above, real-time 3D echocardiography will be used instead of 2D echocardiography in clinical situation. First of all, it is free from IP error because during scanning, the whole objects can be scanned through at different orientations and only the acquisition of a single volume is required, thus there will not be the problems of improper planes to be imaged [9]. Besides, since a large number of cross sections is imaged, ample planes can be taken account for volume calculation (summation of multiplying the appropriate cross-sectional areas with the section thickness) so that the reliance on geometric assumption can be reduced. As a result, GA error will be small.

On the other hand, MRI is seldom used in clinical situation because it is too expensive and real-time measurement of the left ventricular volume during cardiac cycle cannot be achieved by using MRI [9].

REFERENCES

[1] Lab manual.
[2] Cobbold, R. S. (2007). Foundations of biomedical ultrasound. Oxford University Press on Demand.
[3] Beutel, J., Kundel, H. L., & Van Metter, R. L. (2000). Handbook of Medical Imaging, volume 1: Physics and Psychophysics.
[4] Hendee, W. R., & Ritenour, E. R. (2003). Medical imaging physics. John Wiley & Sons.
[5] Helak, J. W., & Reichek, N. (1981). Quantitation of human left ventricular mass and volume by two-dimensional echocardiography: in vitro anatomic validation. Circulation, 63(6), 1398-1407.
[6] Folland, E. D., Parisi, A. F., Moynihan, P. F., Jones, D. R., Feldman, C. L., & Tow, D. E. (1979). Assessment of left ventricular ejection fraction and volumes by real-time, two-dimensional echocardiography. A comparison of cineangiographic and radionuclide techniques. Circulation, 60(4), 760-766.
[7] King, F. W. (2009). Hilbert transforms (Vol. 2). Cambridge, United Kingdom: Cambridge University Press.
[8] Thomas L.Szabo. (2013) Diagnostic Ultrasound Imaging: Inside out. 2nd Edition. Academic Press.

[9] Chukwu, E. O., Barasch, E., Mihalatos, D. G., Katz, A., Lachmann, J., Han, J., & Gopal, A. S. (2008). Relative importance of errors in left ventricular quantitation by two-dimensional echocardiography: insights from three-dimensional

echocardiography and cardiac magnetic resonance imaging. *Journal of the American Society of Echocardiography*, *21*(9), 990-997.

[10] Benzarti, F., & Amiri, H. (2013). Speckle noise reduction in medical ultrasound images. *arXiv preprint arXiv:1305.1344*.

[11] Helak, J. W., & Reichek, N. (1981). Quantitation of human left ventricular mass and volume by two-dimensional echocardiography: in vitro anatomic validation. Circulation, 63(6), 1398-1407.

Appendix:

1.1

```
[B_1,header_1]=RPread_WL('1.b8');
[B_2,header_2]=RPread_WL('2.b8');
[B_3,header_3]=RPread_WL('3.b8');
[B_4,header_4]=RPread_WL('4.b8');
resol=45/356;
y_B=[0 resol*356];
x_B=[0 resol*488];
figure, imagesc(x_B,y_B,B_1(:,:,70)), colormap(gray),
title('Fig 1'), xlabel('(mm)'), ylabel('(mm)'),colorbar, axis
equal;
figure, imagesc(x_B,y_B,B_2(:,:,70)), colormap(gray),
title('Fig 2'), xlabel('(mm)'), ylabel('(mm)'),colorbar, axis
equal;
figure, imagesc(x_B,y_B,B_3(:,:,70)), colormap(gray),
title('Fig 3'), xlabel('(mm)'), ylabel('(mm)'),colorbar, axis
equal;
figure, imagesc(x_B,y_B,B_4(:,:,70)), colormap(gray),
title('Fig 4'), xlabel('(mm)'), ylabel('(mm)'),colorbar, axis
equal;
```

1.2

```
[Im,header_Im]=RPread_WL('group5.rf');
[Bmode,header_B]=RPread_WL('group5.b8');
Im_hilbert_line=hilbert(Im(:,100,87));
figure, plot(abs(Im_hilbert_line),'r');
hold on;
plot(Im(:,100,87),'b');
hold off;
xlim([500 1000]);

resol=45/356;

y_B=[0 resol*356];
x_B=[0 resol*488];

figure, imagesc(x_B,y_B,Bmode(:,:,87)), colormap(gray),
title('Bmode'), xlabel('(mm)'), ylabel('(mm)'),colorbar, axis
equal;
figure, imagesc(Im(:,:,87)), colormap(gray), title('raw rf'),
colorbar;
Im_hilbert=hilbert(Im(:,:,87));
figure, imagesc(abs(Im_hilbert)), colormap(gray),
title('Hilbert'), colorbar;
Im_hilbert_scale=20*log10(abs(Im_hilbert));
figure, imagesc(Im_hilbert_scale), colormap(gray),
title('Hilbert scaled'), colorbar;
[transverse,header_T]=RPread_WL('zachTransverse.b8');
figure, imagesc(x_B,y_B,transverse(:,:,50)),
colormap(gray), title('Transverse Plane'), xlabel('(mm)'),
ylabel('(mm)'),colorbar, axis equal;
```

1.3

```
header_B =
   filetype: 4
    nframes: 87
          w: 488
          h: 356
         ss: 8
         ul: [101 9]
         ur: [387 9]
         br: [387 347]
         bl: [101 347]
      probe: 2
        txf: 6666666
         sf: 0
         dr: 23
         ld: 0
      extra: 133
```

Transverse:

```
header_T =
   filetype: 4
    nframes: 50
          w: 488
          h: 356
         ss: 8
         ul: [101 9]
         ur: [387 9]
         br: [387 347]
         bl: [101 347]
      probe: 2
        txf: 6666666
         sf: 0
         dr: 23
         ld: 0
      extra: 133
```

2.1

```
img = abs(sos(ifft2c(ReorderData1(:,:,:,6)),3));
img_c = img;
for n= 1:11
```

```
    z= n*1.5*2-3;
    str=sprintf('z = %0.5gmm',z);
    figure,imagesc([0 32],[0
32],abs(sos(ifft2c(ReorderData1(:,:,:,n)),3))),colormap(gra
y),title(str),xlabel('mm'), ylabel('mm');axis equal;

    z= n*1.5*2-1.5;
    str=sprintf('z = %0.5gmm',z);
    figure,imagesc([0 32],[0
32],abs(sos(ifft2c(ReorderData1(:,:,:,n+12)),3))),colormap(
gray),title(str),xlabel('mm'), ylabel('mm');axis equal;

end
```

2.2

```
img_c= abs(sos(ifft2c(ReorderData1(:,:,:,1)),3));
figure, imagesc(img_c), title('original
image'),colormap(gray);
[~, threshold] = edge(img_c, 'sobel');
fudgeFactor = 0.6;
BWs = edge(img_c,'sobel', threshold * fudgeFactor);
figure, imshow(BWs), title('binary gradient mask');
se90 = strel('line', 6, 90);
se0 = strel('line', 6, 0);
BWsdil = imdilate(BWs, [se90 se0]);
figure, imshow(BWsdil), title('dilated gradient mask');
BWdfill = imfill(BWsdil);
% double click area to be filled
figure, imshow(BWdfill);
title('binary image with filled holes');
seD = strel('diamond',1);
BWFinal = imerode(BWdfill,seD);
BWFinal = imerode(BWFinal,seD);
figure, imshow(BWFinal);
title('final segmented image');
label=bwlabel(BWFinal);
stats = regionprops(label);
areas = [stats.Area];
[maxArea index] = max(areas);
figure, imshow(label==index);
maxArea
```